Explosive volcanic eruptions from linear vents on Earth, Venus and Mars: Comparisons with circular vent eruptions

Lori S. Glaze[1], Stephen M. Baloga[2], and Jesse Wimert[3]

[1] NASA's Goddard Space Flight Center
Greenbelt, MD 20771
Lori.S.Glaze@nasa.gov

[2] Proxemy Research
20528 Farcroft Lane
Gaithersburg, MD 20882
Steve@Proxemy.com

[3] University of Maryland
Department of Astronomy
College Park, MD 20742
jwimert@umd.edu

Revised for JGR/Planets

9/29/10

Abstract: Conditions required to support buoyant convective plumes are investigated for explosive volcanic eruptions from circular and linear vents on Earth, Venus, and Mars. Vent geometry (linear versus circular) plays a significant role in the ability of an explosive eruption to sustain a buoyant plume. On Earth, linear and circular vent eruptions are both capable of driving buoyant plumes to equivalent maximum rise heights, however, linear vent plumes are more sensitive to vent size. For analogous mass eruption rates, linear vent plumes surpass circular vent plumes in entrainment efficiency approximately when $L_o \geq 3r_o$ owing to the larger entrainment area relative to the control volume. Relative to circular vents, linear vents on Venus favor column collapse and the formation of pyroclastic flows because the range of conditions required to establish and sustain buoyancy is narrow. When buoyancy can be sustained, however, maximum plume heights exceed those from circular vents. For current atmospheric conditions on Mars, linear vent eruptions are capable of injecting volcanic material slightly higher than analogous circular vent eruptions. However, both geometries are more likely to produce pyroclastic fountains, as opposed to convective plumes, owing to the low density atmosphere. Due to the atmospheric density profile and water content on Earth, explosive eruptions enjoy favorable conditions for producing sustained buoyant columns, while pyroclastic flows would be relatively more prevalent on Venus and Mars. These results have implications for the injection and dispersal of particulates into the planetary atmosphere and the ability to interpret the geologic record of planetary volcanism.

1. Introduction

The mechanisms by which ash and volatiles are transported by explosive volcanism on Venus and Mars are important issues that relate to present day observations of the surface and the

64 evolution of the climate, atmospheric chemistry and subsurface conditions. Advances in
65 understanding the range of magma compositions on Mars [*e.g.*, *Rieder et al.*, 1997; *Bandfield et*
66 *al.*, 2000] continue to expand notions of the prevalence of extensive explosive volcanism.
67 Detection of elevated SO_2 in the upper atmosphere of Venus [*Esposito*, 1984; *Moore et al.*, 1992;
68 *Robinson et al.*, 1995; *Glaze*, 1999] and diffuse deposits near the summits of some volcanoes
69 [*Campbell and Rogers*, 1994] also seem consistent with explosive volcanism.

70 There is abundant geologic evidence on both Venus and Mars for large volume volcanic
71 eruptions from long linear vent systems (e.g., Figure 1). Extensive flood volcanism and very long
72 duration fissure eruptions have been conjectured to have played an important role in the
73 formation of many units and features on Mars (e.g., *Greeley and Spudis* [1981]; *Keszthelyi et al.*
74 [1999]; *Greeley et al.* [2000]; *Keszthelyi et al.* [2006]). It is becoming increasingly evident that
75 this form of volcanism is also important for Venus. Roughly 20% of the large flow fields on
76 Venus originate from fractures (e.g., Figure 1b) [*Stofan and Smrekar*, 2005], and clearly fall into
77 the flood lava category, with areal extents ranging from 39,000 to 744,000 km^2 [*Magee and*
78 *Head*, 2001], and thickness estimates ranging from <100 m to 1 km [*Roberts et al.*, 1992;
79 *Lancaster et al.*, 1995]. Terrestrial flood basalt eruptions, such as the Roza eruption of the
80 Columbia River Basalt Group and those associated with the Deccan province, have been
81 responsible for significant volatile degassing with associated impacts on climate [*Thordarson*
82 *and Self*, 1996; *Self et al.*, 2006]. However, studies that deal with the volcanic contribution of
83 volatiles into planetary atmospheres [*Greeley*, 1987; *Wilson and Mouginis-Mark*, 2001] have
84 given only limited attention to the ability of plumes associated with explosive phases of large
85 effusive eruptions to transport and disperse volatiles and ash.

86 Buoyant plumes rising above basaltic fissure eruptions on Earth are well documented [e.g.,
87 *Thordarson and Self*, 1993; *Walker et al.*, 1984; *Lockwood et al.*, 1984; *Thordarson and Larson*,
88 2007]. Terrestrial experience [*Thorarinson*, 1969; *Carracedo et al.*, 1992; *Thordarson and Self,*
89 *1993*] indicates that fissure eruptions typically comprise multiple effusive and explosive
90 episodes. These episodes commonly involve localized activity along various sub-sections of the
91 fissure as the eruption progresses. Active fissure lengths for historical eruptions range from a few
92 hundred meters (e.g, 1961 eruption of Askja, Iceland [*Thorarinson and Sigvaldason*, 1962], to a
93 few kilometers (e.g., 1886 eruption of Tarawera, New Zealand [*Walker et al.*, 1984], and 1783
94 eruption of Laki [*Thordarson and Self*, 1993]). The surface expression of fissure vents on Venus
95 and Mars are often tens of km in length. The fissure segment shown in Figure 1a is just part of
96 the overall fissure. Concentric fissures, like those at Alba Patera, are an order of magnitude
97 larger. In addition, volume eruption rates may have been orders of magnitude larger than
98 terrestrial analogs [*Wilson and Mouginis-Mark*, 2001; *Baloga et al.*, 2003; *Baloga and Glaze,*
99 2008]. Although volcanic fissures visible on the surface of Venus or Mars were not likely active
100 along their entire length at any one time, large conjectured volumetric eruption rates may point to
101 active fissure lengths significantly greater than the documented terrestrial analogs.
102 Over the last 30 years, there have been numerous models for explosive volcanic eruption
103 columns based on the ideas for buoyant, convecting plumes presented by *Morton et al.* [1956]
104 (e.g., *Wilson* [1976]; *Wilson et al.* [1978]; *Woods* [1988]; *Stothers* [1989]; *Thornhill* [1993];
105 *Woods* [1993b] *Glaze et al.* [1997]; *Glaze* [1999]; *Hort and Weitz* [2001]). However, with the
106 exception of *Stothers* [1989] and *Woods* [1993a], the effects of linear geometry (including
107 multiple aligned point sources) on plume dynamics have largely been ignored. In general,
108 volcanic plume models have focused on eruptions from localized circular vents under the

109 assumption that linear vent plumes that rise much higher than the length of active fissure can be
110 approximated with a point source. The original basis for this assumption was the field work by
111 *Walker et al.* [1984] on the 1886 fissure eruption of Tarawera, the largest historical eruption in
112 New Zealand, where most of the erupted material originated from a series of closely space vents
113 along a 7 km fissure. During its most explosive phase, a Plinian plume rose to an estimated
114 height of 28 km above a 4 km active segment of the fissure. The distal airfall deposit from this
115 Plinian plume exhibits a symmetry consistent with (i.e., indistinguishable from) fallout from a
116 plume originating from a circular vent. *Walker et al.* [1984] infer from the surface distribution of
117 distal ash that, because the rise height was so much greater than the active fissure length, the
118 plume material "forgot" that it originated from an extended source. However, this inference
119 derives from the final surface deposit, and as such, reflects more on the processes that influence
120 settling rather than vertical transport. It ignores the dynamic transport characteristics that might
121 be associated with different vent geometries and the ability of a plume to transport material up to
122 a diffusive regime.

123 It is not at all unexpected that some component of the fallout deposit from a large linear vent
124 eruption should be more symmetric in nature. First, for narrow linear plumes, most of the
125 entrainment occurs along the linear extent of the plume, and thus expansion perpendicular to the
126 fissure axis is dominant. Expansion parallel to the fissure axis should be small in comparison.
127 Thus, by the time a plume reaches heights such as 28 km, the expansion of the plume may well
128 be more circular in nature. Second, atmospheric diffusion and turbulence during ash fallout
129 [*Suzuki,* 1983; *Armienti et al.,* 1988; *Glaze and Self,* 1991] produce a randomizing effect on the
130 final deposition of ash on the surface, smoothing and masking (i.e., "forgetting") the original
131 linear nature of the plume rise. However, *Walker et al.* [1984] also noted that the thickness of the

132 proximal airfall deposit did not vary much with distance along the 4 km active segment of the
133 fissure. From this observation, they concluded that the entire 4 km fissure segment was likely
134 active concurrently. This observation directly supports the inference that the linear vent
135 geometry is important to the dynamics of the plume transporting the material found in the
136 proximal deposit. Thus, dynamics of plume rise, particularly in the first few kilometers, may be
137 significantly influenced by the vent geometry.

138 Key issues for planetary explosive volcanism include the heights attainable by convecting
139 plumes, the ability to transport and disperse particulates and volatiles, and the subsurface
140 conditions within the feeding conduit required to sustain a column. All the models based on
141 extensions of the *Morton et al.* [1956] system of equations indicate that atmospheric entrainment
142 in the first few kilometers of the eruption column play a dominant role in the dynamics of
143 buoyant plumes. Entrainment, in turn, depends upon the surface area and upward velocity of the
144 plume in the lower reach.

145 In this paper, quantitative constraints are developed for the dimensions and character of
146 buoyant columns for a range of active linear and circular vent systems and eruption conditions
147 on the Earth, Venus, and Mars. The influence of atmospheric profile, gravity, geometric and
148 scale differences among these planets are evaluated. This is accomplished by adapting previous
149 models for buoyant plumes arising from central vents [*Glaze and Baloga*, 1996; *Glaze et al.*,
150 1997; *Glaze 1999*; *Glaze and Baloga*, 2002] to linear vent geometries. The models used in this
151 work are analogous to the more elementary single-component linear source model of *Stothers et*
152 *al.* [1986] and *Stothers* [1989] with the adaptation to both solid and vapor plume constituents.
153 The results obtained in this paper provide significant implications for the relative roles of

154 widespread airfall and pyroclastic flow mechanisms in forming the geologic record from
155 explosive volcanism on the terrestrial planets.

156 2. Convective Plume Model

157 The approach to modeling linear volcanic vents described here builds on the original work by
158 *Stothers* [1989] but takes advantage of substantial improvements that have been made in
159 volcanic plume modeling over the last 20 years. Changes from the *Stothers* [1989] approach
160 include (1) explicit inclusion of the conservation of thermal energy, as proposed by *Woods*
161 [1988], and implemented by *Glaze and Baloga* [1996], *Glaze et al.* [1997], *Glaze* [1999] and
162 *Glaze and Baloga* [2002], (2) consideration of multiple plume components, particularly solids,
163 and (3) more detailed information on Venus and Mars atmospheric compositions.

164 In general, the complete system of equations describing buoyant plume rise that must be
165 solved requires at least a half dozen differential equations and another half dozen equations
166 describing parameters within the plume and ambient atmosphere. Table 1 shows the system of
167 differential equations from *Glaze et al.* [1997] where the control volume and entraining area are
168 given in a generic form in the first column (Notation is defined in Table 2). For the cylindrically
169 axisymmetric system in *Glaze et al.* [1997], shown in Figure 2a, the control volume is defined as
170 $V = \pi r^2 dz$, and the area through which ambient is entrained is $A_e = 2\pi r\, dz$. For the linear vent
171 system shown in Figure 2b, $V = 2bLdz$ and $A_e \approx 2Ldz$ (where it is assumed that $L >> b$). The
172 approach is then to solve the sets of governing equations in Table 1 for both central and linear
173 vent geometries. The results described below have assumed that L remains relatively constant as
174 a function of z. Thus L does not appear in any of the linear vent conservation equations in Table
175 1.

176 Boundary conditions at the vent for all variables (r, b, u, θ, and n) are denoted by a

177 subscripted "o". The vent is defined as the top of the feeding conduit, and the point at which the
178 erupted material is free to entrain ambient atmosphere and expand. Note that the dimensions at
179 the top of the conduit can be considerably smaller than the visible expression of the vent at the
180 surface for both circular and linear vents. Values for the entrainment constant, α, have been
181 estimated for buoyant plumes originating from both circular and linear vents using empirical
182 [e.g., Batchelor, 1954; Morton et al., 1956], theoretical [Agrawal and Prasad, 2003], and
183 simulation [Suzuki and Koyaguchi, 2010] approaches. Values for circular vent plumes range
184 from 0.05 – 0.15, and from 0.0975 – 0.16 for linear vent plumes. For the purpose of comparing
185 the effects of geometry only, this study assumes a value of $\alpha = 0.09$ for all cases.

186 In addition to the conservation equations defined by (3) – (8), the system is completed by the
187 following definitions for volume fraction,

188 $$\phi_d + \phi_v + \phi_s = 1 \qquad (9)$$

189 the ideal gas law,

190 $$P = \left(\rho_d \phi_d R_d + \rho_v \phi_v R_v\right)\theta \qquad (10)$$

191 bulk density,

192 $$\rho_B = \rho_d \phi_d + \rho_v \phi_v + \rho_s \phi_s \qquad (11)$$

193 and the bulk specific heat,

194 $$C_B = \left[\rho_d \phi_d C_a + \rho_v \phi_v C_v + \rho_s \phi_s C_s\right] / \rho_B \qquad (12)$$

195 Following *Glaze and Baloga* [1996], *Glaze et al.* [1997], *Glaze* [1999] and *Glaze and Baloga*
196 [2002], the systems of ordinary differential equations in Table 1 are solved simultaneously using
197 a Runge-Kutta technique. To avoid numerical artifacts in the boundary region near the plume
198 top, the maximum plume height is defined as the height at which the upward velocity drops to

199 below 10 m/s. Plume rise beyond this point is minimal (relative to the overall plume height),
200 while the velocity drops quickly and the corresponding plume radius (or half width for linear
201 plumes) increases exponentially.
202

203 ## 3. Results for Earth's Atmosphere

204 Much has been published on the sensitivities of the central vent model given in Table 1 [e.g.,
205 *Wilson,* 1976; *Wilson et al.*, 1978; *Woods*, 1988; *Glaze and Baloga,* 1996; *Glaze et al.*, 1997].
206 Thus, here, the focus is on the primary differences that result from the linear vent geometry
207 relative to the central vent. The numerical code used to solve the linear vent system is identical to
208 the central vent model, where the only differences are those resulting from the geometry of the
209 vents.

210 Figure 3 illustrates a basic comparison of predicted plume heights on Earth for a range of
211 vent sizes. As noted above, the length of fissure vent that is active does not appear in the
212 conservation equations in Table 1. Thus, a simple comparison can be made of plume height as a
213 function of either b_o (for linear vents) or r_o (for circular vents). For the results shown in Figure 3,
214 all of the boundary values at the vent are kept the same, except for the size of the vent opening
215 (radius, r_o, for circular vents, or half-width, b_o, for linear vents). The vent conditions used for
216 both geometries are velocity, u_o = 300 m s^{-1}, temperature, θ_o = 1000 K, and the mass fraction of
217 water vapor, n_o = 0.03, where the mass fraction of vapor in the plume is defined as $n = \rho_V \phi_V / \rho_B$.
218 For this example, the plumes are assumed to rise from sea level into the US Standard atmosphere
219 (e.g., *Wallace and Hobbs* [1977]).

220 For this set of boundary conditions both the linear and circular vent models produce a
221 maximum plume height of around 35 km. Figure 3 shows maximum plume heights for circular

222 and linear vents, plotted for a broad range of vent sizes. From this plot, it can be seen that
223 buoyant, convecting plumes originating from circular vents can be maintained with substantial
224 maximum heights over a wide range of vent sizes, from a radius of a few meters to around 900
225 meters. For the boundary conditions used in this analysis, plumes from circular vents collapse, or
226 are otherwise unable to maintain a steady column, for vent sizes greater than about 900 m.
227 However, the linear plumes are much more sensitive to the vent size, and can maintain a
228 convective plume over a much more narrow range of vent sizes. For the same boundary
229 conditions (temperature, velocity, gas mass fraction), plumes from linear vents only reach
230 significant heights for values of b_o of a few meters to ~200 meters. For this set of boundary
231 conditions, the peak plume height occurs when $b_o \approx 75$ m.

232 Because one of the main drivers of plume height is the mass flux at the vent [*Woods,* 1988;
233 *Glaze and Baloga*, 1996], a better comparison between linear and circular vents can be made by
234 examining predicted plume heights for equivalent mass fluxes. The mass flux at the vent is
235 defined as the density of the erupted material multiplied by the cross sectional area of the vent
236 and the exit velocity (= $\rho_{Bo} u_o A_o$). Keeping the bulk plume density and exit velocities the same
237 for both linear and circular vents, the key parameter for comparison becomes the cross sectional
238 vent area, where $A_o = \pi r_o^2$ for the circular vent, and $A_o = 2 b_o L_o$ for the linear vent.

239 Column 1 of Table 3 indicates a range of cross sectional vent areas. Column 2 of Table 3
240 contains the corresponding radii for circular vents. For linear vents, the half-width, b_o,
241 corresponding to the cross sectional area is dependent upon the choice for active fissure length,
242 L_o. Noting that the original definition of a linear vent included the assumption that $L_o >> b_o$, the
243 table only considers values for b_o that are less than an order of magnitude smaller than L_o. Active
244 fissure lengths up to 10 km are considered.

245 Figure 4 illustrates the plume heights corresponding to the vent sizes given in Table 3. From
246 Figure 4, it can be seen that as L_o increases, linear plumes become more capable of establishing a
247 convective regime over a broad range of b_o, similar to the circular vents. This is primarily
248 because as L_o increases, the entrainment area of the linear plumes increases relative to the control
249 volume. The ability of a plume to become buoyant is driven by whether or not sufficient air can
250 be entrained (and warmed) to reduce the bulk plume density before upward momentum is
251 exhausted. From the right hand side of (3) the mass of dry air entrained by the linear plume is
252 roughly the same as the cylindrical case when $uL \approx \pi ur$. Thus, the linear plumes surpass circular
253 vents in entrainment efficiency approximately when $L_o \geq 3r_o$. Note, however, that because L does
254 not appear in the governing equations, the maximum plume height in Figure 4 always occurs
255 around $b_o \approx 75$ m.
256

257 ## 4. Applications to Venus and Mars

258 Analysis of the linear vent model under ambient conditions found on Venus and Mars are
259 now considered. Because of the extreme differences in the atmospheric densities, boundary
260 condition values used in these analyses are slightly different than those used for Earth.
261 For comparison with conditions considered by *Glaze* [1999], the variables held constant
262 under Venus conditions are the initial velocity, $u_o = 270$ m s^{-1}, initial temperature, $\theta_o = 1400$ K,
263 and the mass fraction of water vapor, $n_o = 0.05$. Further, the scenarios discussed here have used
264 the high latitude atmospheric temperature and pressure profile [*Seiff et al.*, 1985], as explosive
265 eruptions under these conditions were shown by *Glaze* [1999] to be the most likely to rise to
266 significant altitudes. The primary difference between the boundary conditions used here and

267 those used by *Glaze* [1999] is that here it has been assumed that the vent is at 0 km above the
268 mean planetary radius (as opposed to 10 km ampr).

269 Figure 5 shows the plume heights reached for circular and linear vents for a range of radii
270 and half widths, respectively. There are several points of interest to note. First, consistent with
271 work by *Thornhill et al* [1993] and *Glaze* [1999], the range of conditions over which buoyant
272 plumes can be maintained on Venus is very narrow (note the range on the x axis is only 300 m,
273 compared to > 800 m on Earth). Also, the shape of the curve for circular vents is substantially
274 different from the terrestrial case, with an almost linear relationship between vent radius and
275 maximum plume height. The primary explanation for this difference in shape is the much higher
276 pressure ambient atmosphere.

277 The maximum plume height achievable for the given boundary conditions is ~52 km
278 corresponding to a circular vent radius of 247 m. Like the terrestrial case, there is a very abrupt
279 break at the point where a convective plume can no longer be maintained. For linear vents, the
280 range of conditions that can maintain a convective plume is likewise very narrow, with the
281 maximum plume height of ~69 km occurring when b_o = 16 m. Unlike the terrestrial case, linear
282 vents on Venus appear capable of driving a plume to somewhat higher maximum altitudes, for
283 all other things remaining equal, albeit under very limited conditions.

284 As for Earth, a better comparison between the circular and linear vents is made by looking at
285 the plume heights for each when the mass flux at the vent (and thus the cross sectional vent area)
286 is the same. Table 4 indicates circular vent radii and linear vent cross widths for a range of cross
287 sectional vent areas. Again, the linear vent half widths are restricted to those that are less than an
288 order of magnitude smaller than the fissure length, consistent with the assumption that $b_o << L_o$.

289 Figure 6 shows the predicted plume heights for the vent sizes given in Table 4. It can be seen
290 that the maximum plume height for the linear vent case occurs consistently for b_o = 16 m, but the
291 peak is shifted to the right by increasing the vent size (i.e., L). Unlike the terrestrial example,
292 however, the linear vent is more effective than its circular counterpart at producing a convective
293 plume that is capable of reaching significant heights for the same mass flux.
294 For Mars, the variables held constant are initial velocity, u_o = 230 m s^{-1}, initial temperature,
295 θ_o = 1000 K, and mass fraction of water vapor, n_o = 0.01. It should be noted that *Glaze and*
296 *Baloga* [2002] placed limits on the applicability of buoyancy models such as the one described
297 here. That study indicated that such models are not valid above heights greater than 10 – 20 km
298 on Mars under current atmospheric conditions. For those boundary conditions that produce
299 plumes higher than about 10 km, the alternative approach of *Wilson and Head* [2007] is used to
300 model the subsequent inertial transport of particles along ballistic trajectories. Using this
301 approach, the upward velocity and plume dimensions at 10 km are used as starting conditions for
302 momentum driven rise. Plume heights found using the convective model are compared to the
303 heights found using the combined buoyancy-ballistic approach for the circular and linear vents in
304 Figure 7.
305 Using the combined buoyancy-ballistic approach, a comparison of the linear and circular
306 vents is made by examining plume heights for fixed mass fluxes (Table 5, Figure 8), as was done
307 for Earth and Venus. The ballistic constraint above 10 km results in no plumes that rise above 15
308 km above the vent. The plumes from circular vents decrease in height as the mass flux (i.e., vent
309 area) increases, implying column collapse conditions. However, in contrast, the linear vent
310 plumes continue to show an increase in maximum plume height as mass flux increases,
311 indicating that the upward velocity of the bulk plume material at 10 km altitude (where transport

312 transitions from convective to ballistic) is also increasing. The implication is, therefore, that
313 these linear vent plumes are not necessarily collapsing, and that linear vent plumes develop a
314 pyroclastic fountain capable of injecting a substantial amount of ash and volatiles into the
315 atmosphere at the plume top.

316 The preference for the formation of pyroclastic flows and near vent deposition on Mars, as
317 opposed to widely dispersed airfall deposits, is consistent with some prior suggestions in the
318 literature. Most notably, interpretations of early volcanic activity (e.g., *Mouginis-Mark et al.*
319 [1988]; *Carr* [2007]) have suggested numerous and extensive pyroclastic flows on the flanks of
320 Alba Patera prior to a transition of late stage effusive volcanism. Similar considerations may
321 apply to incised units thought to be either airfall or pyroclastic flow deposits at Hecates Tholus
322 and Hadriaca and Tyrrhena paterae [*Mouginis-Mark et al.,* 1982; *Greeley and Crown,* 1990;
323 *Gregg and Farley,* 2006].
324

325 ## 5. Conclusions

326 When buoyancy can be sustained, plumes from both linear and circular volcanic vents have
327 very similar maximum heights. However, the conditions required to sustain buoyant plumes are
328 highly restricted for linear vents. The range of conditions for sustained buoyancy is very narrow
329 for Venus and relatively more favorable for the Earth. The dependence of maximum plume
330 height on circular vent diameter is dominated by the nature of the ambient atmospheric profiles
331 for density, pressure, and water content. On Venus, the extreme ambient atmospheric pressures
332 (100 times Earth) result in an almost linear relationship between the vent radius and plume
333 height.

When buoyancy is sustained, linear vents appear to be equally capable of injecting volcanic ash and volatiles into the atmosphere. For analogous mass flux rates at the vent, the maximum heights to which linear and cylindrical plumes can rise are essentially equivalent. In cases where the length of active linear vent is less than approximately $3r_o$, the entrainment area of linear plumes is significantly less than the cylindrical (circular vent) equivalent. Thus the range of vent widths that can sustain a buoyant plume is narrow and these plumes are more likely to collapse.

Only the Earth, with its thick wet atmosphere, favors explosive eruptions that can maintain convective plumes reaching 10s of km in altitude. Conversely, the range of plausible conditions that can produce a buoyant convective plume on Venus is very restricted. The probability of an eruption occurring with just the right boundary conditions is relatively small. Thus, it seems that pyroclastic flows are much more likely in the nonterrestrial environments. On Mars, the results presented here favor interpretations of pyroclastic flows and near vent deposition at major volcanic centers, including Alba, Hadriaca, and Tyrrhena paterae and Hecates tholus, where the discriminating morphologic diagnostics remain ambiguous.

6. Acknowledgements

This work was funded by the NASA Planetary Geology and Geophysics Program (WBS 811073.02.01.04.44 for L. Glaze, and Grant #NNX08AF16G for S. Baloga). J. Wimert was supported by L. Glaze (Planetary Geology and Geophysics WBS) through the University of Maryland CRESST program. The authors would like to thank Steve Self for a very constructive review of this manuscript.

356 **References**

357 Agrawal, A., and A.K. Prasad, Integral solution for the mean flow profiles of turbulent jets,
358 plumes and wakes, Journal of Fluids Engineering, 125, 813 - 822, 2003.
359 Armienti, P., G. Macedonio, and M.T. Pareschi, A numerical model for simulation of tephra
360 transport and deposition; applications to May 18, 1980, Mount St. Helens eruption, Journal
361 of Geophysical Research, 93 (6), 6463-6476, 1988.
362 Baloga, S.M., and L.S. Glaze, A Self-replication model for long channelized lava flows on the
363 Mars plains, Journal of Geophysical Research, submitted (6/07), 2008.
364 Baloga, S.M., P.J. Mouginis-Mark, and L.S. Glaze, Rheology of a long lava flow at Pavonis
365 Mons, Mars, Journal of Geophysical Research, 108 (E7), 5066, 2003.
366 Banfield, J.L., V.E. Hamilton, and P.R. Christensen, A global view of Martian surface
367 compositions from MGS-TES, *Science, 287*, 1626 - 1630, 2000.
368 Batchelor, G.K., Heat convection and buoyancy effects in fluids, Quart. J. R. Met. Soc., 80, 339 -
369 358, 1954.
370 Campbell, B.A., and P.G. Rogers, Bell Regio, Venus; integration of remote sensing data and
371 terrestrial analogs for geologic analysis, *Journal of Geophysical Research, 99* (E10), 21,153-
372 21,171, 1994.
373 Carr, M.H., *The Surface of Mars*, 322 pp., Cambridge University Press, Cambridge, 2007.
374 Carracedo, J.C., E. Rodriguez Badiola, and V. Soler, The 1730 - 1736 eruption of Lanzarote,
375 Canary Islands: a long, high-magnitude basaltic fissure eruption, J. Volcanol. Geotherm.
376 Res., 53, 239 - 250, 1992.
377 Esposito, L.W., Sulfur Dioxide: Episodic injection shows evidence for active Venus volcanism,
378 *Science*, *223*, 1072 - 1074, 1984.

379 Glaze, L., S.M. Baloga, and L. Wilson, Transport of atmospheric water vapor by volcanic
380 eruption columns, *Journal of Geophysical Research, 102* (D5), 6099-6108, 1997.
381 Glaze, L.S., and S. Baloga, Volcanic plume heights on Mars: Limits of validity for convective
382 models, *Journal of Geophysical Research, 107* (E10, 5086), doi:10.1029/2001JE001830,
383 2002.
384 Glaze, L.S., and S.M. Baloga, Sensitivity of buoyant plume heights to ambient atmospheric
385 conditions: Implications for volcanic eruption columns, *Journal of Geophysical Research,*
386 *101* (D1), 1529-1540, 1996.
387 Glaze, L.S., and S. Self, Ashfall dispersal for the 16 September 1986, eruption of Lascar, Chile,
388 calculated by a turbulent diffusion model, Geophysical Research Letters, 18 (7), 1237-1240,
389 1991.
390 Glaze, L.S., Transport of SO_2 by explosive volcanism on Venus, *Journal of Geophysical*
391 *Research, 104* (E8), 18,899 - 18,906, 1999.
392 Greeley, R., and P.D. Spudis, Volcanism on Mars, *Reviews of Geophysics and Space Physics, 19*
393 (1), 13-41, 1981.
394 Greeley, R., N.T. Bridges, D.A. Crown, L.S. Crumpler, S.A. Fagents, P.J. Mouginis-Mark, and J.
395 Zimbelman, Volcanism on the Red Planet: Mars, in *Environmental Effects on Volcanic*
396 *Eruptions: From Deep Oceans to Deep Space*, edited by J. Zimbelman, and T.K.P. Gregg,
397 pp. 75, Kluwer Academic/Plenum Publishers, New York, 2000.
398 Greeley, R., Release of juvenile water on Mars; estimated amounts and timing associated with
399 volcanism, *Science, 236* (4809), 1653-1654, 1987.
400 Greeley, R. and D. Crown, Volcanic geology of Tyrrhena Patera, Mars, J. Geophys. Res., 95
401 (B5), 7133 – 7149, 1990.

402 Gregg, T.K.P. and M.A. Farley, Mafic pyroclastic flows at Tyrrhena Patera, Mars: Constraints
403 from observations and models, J. Volcanol. Geotherm. Res., 155, 81 – 89, 2006.
404 Hort, M., and C.M. Weitz, Theoretical modeling of eruption plumes on Mars under current and
405 past climates, *Journal of Geophysical Research, 106* (9), 20,547-20,562, 2001.
406 Keszthelyi, L., S. Self, and T. Thordarson, Application of recent studies on the emplacement of
407 basaltic lava flows to the Deccan Traps, *Memoirs-Geological Society of India, 43*, 485 - 520,
408 1999.
409 Keszthelyi, L., S. Self, and T. Thordarson, Flood lavas on Earth, Io and Mars, *Journal of the*
410 *Geological Society, 163*, 253 - 264, 2006.
411 Lancaster, M., J.E. Guest, and K.P. Magee, Great lava flow fields on Venus, *Icarus, 118*, 69 - 86,
412 1995.
413 Lockwood, J.P., et al., Mauna Loa Volcano, Hawaii, SEAN Bulletin, Smithsonian Institution, 9
414 (3), 2-9, 1984.
415 Magee, K., and J.W. Head, Large flow fields on Venus: Implications for plumes, rift
416 associations, and resurfacing, *Geologic Society of America Special Paper, 352*, 81 - 101,
417 2001.
418 Moore, H.J., J.J. Plaut, P.M. Schenk, and J.W. Head, An unusual volcano on Venus, *Journal of*
419 *Geophysical Research, 97* (E8), 13,479 - 13,493, 1992.
420 Morton, B.R., S.G. Taylor, and J.S. Turner, Turbulent gravitational convection from maintained
421 and instantaneous sources, *234*, 1-23, 1956.
422 Mouginis-Mark, P.J., and P.R. Christensen, New observations of volcanic features on Mars from
423 the THEMIS instrument, *Journal of Geophysical Research, 110*, doi:10.1029/2005JE002421,
424 2005.

425 Mouginis-Mark, P., L. Wilson, and J. Head III, Explosive volcanism on Hecates Tholus, Mars:
426 Investigation of eruption conditions, J. Geophys. Res., 87 (B12) 9890 – 9904, 1982.
427 Mouginis-Mark, P.J., L. Wilson, and J. Zimbelman, Polygenic eruptions on Alba Patera, Mars,
428 *Bulletin of Volcanology, 50* (6), 361 - 379, 1988.
429 Rieder, R., T. Economou, H. Wanke, A. Turkevich, J.A. Crisp, J. Bruckner, G. Dreibus, and
430 H.Y. McSween, The chemical composition of Martian soil and rocks returned by teh mobile
431 Alpha Proton X-ray Spectrometer: Preliminary results from the X-ray mode, *Science, 278*
432 (1771), doi:10.1126/science.278.5344.1771, 1997.
433 Roberts, K.M., J.E. Guest, J.W. Head, and M.G. Lancaster, Mylitta Fluctus, Venus: Rift-related
434 centralized volcanism and the emplacement of large-volume flow units, *Journal of*
435 *Geophysical Research, 97*, 15,991 - 16,015, 1992.
436 Robinson, C.A., G.D. Thornhill, and E. Parfitt, Large-scale volcanic activity at Maat Mons: Can
437 this explain fluctuations in atmospheric chemistry observed by Pioneer Venus?, *Journal of*
438 *Geophysical Research, 100* (E6), 11,755 - 11,763, 1995.
439 Seiff, A., J.T. Schofield, A.J. Kliore, F.W. Taylor, S.S. Limaye, H.E. Revercomb, L.A.
440 Sromovsky, V.V. Kerzhanovich, V.I. Moroz, and M.Y. Marov, Models of the structure of the
441 atmosphere of Venus from the surface to 100 kilometers altitude, *Adv. Space Res., 5* (11), 3 -
442 58, 1985.
443 Self, S., M. Widdowson, T. Thordarson, and A.E. Jay, Volatile fluxes during flood basalt
444 eruptions and potential effects on the global environment: A Deccan perspective, Earth and
445 Planetary Science Letters, 248, 518 - 532, 2006.
446 Stofan, E.R., and S.E. Smrekar, Large topographic rises, coronae, large flow fields and large
447 volcanoes on Venus: Evidence for mantle plumes?, in *Mantle Plume IV Penrose Conference,*

448 pp. 388, Geological Society of America Special Publication, 2005.
449 Stothers, R.B., Turbulent atmospheric plumes above line sources with an application to volcanic
450 fissure eruptions on the terrestrial planets, *Journal of Atmospheric Sciences*, *46* (17), 2662-
451 2670, 1989.
452 Stothers, R.B., J. Wolff, S. Self, and M.R. Rampino, Basaltic fissure eruption plume heights and
453 atmospheric aerosols, Geophysical Research Letters, 13 (8), 725-728, 1986.
454 Suzuki, T., A theoretical Model for Dispersion of Tephra, Arc. Volcanism: Physics and
455 Tectonics, 95-113, 1983.
456 Suzuki, Y.J., and T. Koyaguchi, Numerical determination of the efficiency of entrainment in
457 volcanic eruption columns, Geophys. Res. Letts., 37 (L05302), doi:10.1029/2009GL042159,
458 2010.
459 Thorarinsson, S., and G.E. Sigvaldason, The eruption of Askja 1962, A preliminary rerpot,
460 American Journal of Science, 260, 641 - 651, 1962.
461 Thorarinsson, S., The Laki eruption of 1783, Bulletin of Volcanology, 33, 910 - 929, 1969.
462 Thordarson, T., and G. Larsen, Volcanism in Iceland in historical time: Volcano types, eruption
463 styles and eruptive history, Journal of Geodynamics, 43, 118 - 152, 2007.
464 Thordarson, T., and S. Self, Sulfur, chlorine and fluorine degassing and atmospheric loading by
465 the Roza eruption, Columbia River Basalt Group, Washington, USA, Journal of Volcanology
466 and Geothermal Research, 74, 49 - 73, 1996.
467 Thordarson, T., and S. Self, The Laki (Skaftár Fires) and Grímsvötn eruptions in 1783-1785,
468 Bulletin of Volcanology, 55, 233-263, 1993.
469 Thornhill, G.D., Theoretical modeling of eruption plumes on Venus, *Journal of Geophysical*
470 *Research*, *98* (E5), 9107 - 9111, 1993.

471 Walker, G.P.L., S. Self, and L. Wilson, Tarawera 1886, New Zealand - A basaltic plinian fissure
472 eruption, J. Volcanol. Geotherm. Res., 21, 61 - 78, 1984.
473 Wallace, J.M., and P.V. Hobbs, Atmospheric Science, An Introductory Survey, 467 pp.,
474 Academic Press, Inc., Orlando, 1977.
475 Wilson, L., and J.W. Head, Explosive volcanic eruptions on Mars: Tephra and accretionary
476 lapilli formation, dispersal and recognition in the geologic record, *Journal of Volcanology*
477 *and Geothermal Research*, *163*, 83 - 97, 2007.
478 Wilson, L., and P.J. Mouginis-Mark, Estimation of volcanic eruption conditions for a large flank
479 event on Elysium Mons, Mars, *Journal of Geophysical Research*, *106* (E9), 20,621-20,628,
480 2001.
481 Wilson, L., Explosive Volcanic Eruptions-III. Plinian Eruption Columns, *J. R. astro. Soc.*, *45*,
482 543-556, 1976.
483 Wilson, L., R.S.J. Sparks, T.C. Huang, and N.D. Watkins, The control of volcanic column
484 heights by eruption energetics and dynamics, *Journal of Geophysical Research*, *83* (B4),
485 1829-1836, 1978.
486 Woods, A.W., The fluid dynamics and thermodynamics of eruption columns, *Bulletin of*
487 *Volcanology*, *50*, 169-193, 1988.
488 Woods, A.W., A Model of the Plumes above basaltic fissure eruptions, Geophysical Research
489 Letters, 20 (12), 1115-1118, 1993a.
490 Woods, A.W., Moist convection and the injection of volcanic ash into the atmosphere, Journal of
491 Geophysical Research, 98 (B10), 17,627-17,636, 1993b.
492
493

Figure Captions

Figure 1. Explosive phases from fissure vents, such as those shown here for (a) Mars (18.1° N 245.3° E; THEMIS visible image V05484014) [*Mouginis-Mark and Christensen*, 2005], and (b) Venus (5.5° S, 206° E, Magellan SAR image) may have contributed significant volatiles to the atmosphere.

Figure 2. Schematic views of (a) circular and (b) linear vent geometries. The control volume for each plume is indicated by the gray shaded volume. The entrainment area is the outer, exposed surface area of the control volume. The volcanic vent in both cases is defined as the top of the conduit. Boundary conditions at the vent are denoted by variables with "o" subscript. Note that for linear vents, L_o is >> b_o, and that L does not change substantially as a function of z.

Figure 3. Maximum predicted plume heights as a function of either vent radius (for circular vents), r_o, or half width (for linear vents), b_o. Models assume terrestrial ambient atmospheric conditions with temperature and pressured defined by the US Standard Atmosphere, u_o = 300 m s^{-1}, θ_o = 1000 K, and n_o = 0.03.

Figure 4. Maximum predicted plume heights as a function of vent area. Model boundary conditions are the same as those in Figure 3. The linear vent results are shown for multiple choices of active fissure length.

Figure 5. Maximum predicted plume heights on Venus as a function of either vent radius (for circular vents), r_o, or half width (for linear vents), b_o. Models assume northern Venus latitude ambient atmospheric conditions, $u_o = 270$ m s^{-1}, $\theta_o = 1400$ K, and $n_o = 0.05$.

Figure 6. Maximum predicted plume heights on Venus as a function of vent area. Model boundary conditions are the same as those in Figure 5. The linear vent results are shown for multiple choices of active fissure length.

Figure 7. Maximum predicted plume heights on Mars as a function of either vent radius (for circular vents), r_o, or half width (for linear vents), b_o. Models assume the current low pressure ambient atmospheric conditions, $u_o = 230$ m s^{-1}, $\theta_o = 1000$ K, and $n_o = 0.01$. (a) Predicted plume heights for circular and linear vents when convective model is allowed to run to its full extent, regardless of inconsistencies and non-physical effects (e.g., expansion rates that exceed the speed of sound). (b) Predicted heights for circular and linear vents when convective model is terminated at 10 km. Upward velocity at 10 km is then used to estimate the maximum height for a purely ballistic vertical trajectory.

Figure 8. Maximum predicted plume heights on Mars as a function of vent area. Model boundary conditions are the same as those in Figure 7. The convective model has been terminated at 10 km (as in Figure 7b) and subsequent rise determined from a ballistic vertical trajectory. The linear vent results are shown for multiple choices of active fissure length.

Table 1. System of generic 1st order partial differential equations for convective rise, after *Glaze et al.* [1997]. The control volume and entrainment area can be defined to accommodate either a circular or linear source. Notation is defined in the Table 2.

Description	Generic Conservation Equation	Central Vent	Linear Vent
(1) control volume	V	$V = \pi r^2 dz$	$V = 2bLdz$
(2) entrainment area	A_e	$A_e = 2\pi r dz$	$A_e \approx 2Ldz$
(3) mass: dry air	$\frac{d}{dz}\left[\rho_d u V \phi_d\right] = \rho_a(\alpha u)A_e$	$\frac{d}{dz}\left[\rho_d u r^2 \phi_d\right] = 2\alpha\rho_a u r$	$\frac{d}{dz}\left[\rho_d u b \phi_d\right] = \alpha\rho_a u$
(4) mass: vapor	$\frac{d}{dz}\left[\rho_v u V \phi_v\right] = 0$	$\frac{d}{dz}\left[\rho_v u r^2 \phi_v\right] = 0$	$\frac{d}{dz}\left[\rho_v u b \phi_v\right] = 0$
(5) mass: solid	$\frac{d}{dz}\left[\rho_s u V \phi_s\right] = 0$	$\frac{d}{dz}\left[\rho_s u r^2 \phi_s\right] = 0$	$\frac{d}{dz}\left[\rho_s u b \varphi_s\right] = 0$
(6) mass: bulk	$\frac{d}{dz}\left[\rho_B u V\right] = \rho_a(\alpha u)A_e$	$\frac{d}{dz}\left[\rho_B u r^2\right] = 2\alpha\rho_a u r$	$\frac{d}{dz}\left[\rho_B u b\right] = \alpha\rho_a u$
(7) momentum	$\frac{d}{dz}\left[\rho_B u^2 V\right] = g(\rho_a - \rho_B)V$	$\frac{d}{dz}\left[\rho_B u^2 r^2\right] = g(\rho_a - \rho_B)r^2$	$\frac{d}{dz}\left[\rho_B u^2 b\right] = g(\rho_a - \rho_B)b$
(8) energy	$\frac{d}{dz}\left[\rho_B u V C_B \theta\right] =$ $\rho_a(\alpha u)C_a\theta_a A_e - \rho_a u g V(\phi_d + \phi_v)$	$\frac{d}{dz}\left[\rho_B u r^2 C_B \theta\right] =$ $2\alpha\rho_a u r C_a\theta_a - \rho_a u r^2 g(\phi_d + \phi_v)$	$\frac{d}{dz}\left[\rho_B u b C_B \theta\right] =$ $\alpha\rho_a u C_a\theta_a - \rho_a u g b(\phi_d + \phi_v)$

544 Table 2. Notation[†]

Variable	Definition
A_o	Cross Sectional Vent Area at the top of the conduit (m^2)
A_e	Entrainment Area (m^2)
b	Linear Plume Half Width (m)
C_a	Specific Heat of Ambient Atmosphere (Earth = 998 J K^{-1} kg^{-1}; Venus = Mars = 835 J K^{-1} kg^{-1})
C_B	Bulk Specific Heat of Plume (J K^{-1} kg^{-1})
C_v	Specific Heat of Water Vapor (= 2000 J K^{-1} kg^{-1})
C_s	Specific Heat of Solid Particles (= 920 J K^{-1} kg^{-1})
g	Gravitational Constant (Earth = 9.8 m s^{-2}; Venus = 8.4 m s^{-2}; Mars = 3.7 m s^{-2})
L	Fissure Length (m)
n	Gas Mass Fraction ($=\rho_v\phi_v/\rho_B$)
P	Pressure (Pa)
r	Cylindrical Plume Radius (m)
R_d	Gas Constant for Ambient Atmosphere (Earth = 287 J K^{-1} kg^{-1}; Venus = Mars = 191 J K^{-1} kg^{-1})
R_v	Gas Constant for Water Vapor (= 461 J K^{-1} kg^{-1})
u	Bulk Rise Velocity (m s-^{1})
V	Control Volume (m^3)
z	Vertical Distance (m)
α	Entrainment Constant (=0.09)
θ	Bulk Plume Temperature (K)
θ_a	Ambient Atmopshere Temperature (K)
ρ_a	Ambient Atmospheric Density (kg m^{-3})
ρ_B	Bulk Plume Density (kg m^{-3})
ρ_d	Density of Entrained Ambient (kg m^{-3})
ρ_v	Density of Water Vapor (kg m^{-3})
ρ_s	Density of Solid Particles (= 1000 kg m^{-3})
ϕ_d	Volume Fraction of Entrained Ambient
ϕ_s	Volume Fraction of Solid Particles
ϕ_v	Volume Fraction of Water Vapor

† "o" subscript indicates a value at the vent, defined as the top of the conduit.

546 Table 3. Comparison of terrestrial vent sizes for circular and linear vents and a range of cross
547 sectional vent areas.

A_o [m^2]	r_o [m]	b_o [m]					
		L_o = 500 m	L_o = 1000 m	L_o = 2000 m	L_o = 3000 m	L_o = 5000 m	L_o = 10000 m
3.14 x 10^2	10	0.314	0.157	0.079	0.052	0.031	0.016
1.96 x 10^3	25	1.96	0.982	0.491	0.327	0.196	0.098
6.36 x 10^3	45	6.36	3.18	1.59	1.06	0.636	0.318
1.54 x 10^4	70	15.4	7.70	3.85	2.57	1.54	0.770
7.07 x 10^4	150	-	35.3	17.7	11.8	7.07	3.53
1.52 x 10^5	220	-	76.0	38.0	25.3	15.2	7.60
2.83 x 10^5	300	-	-	70.7	47.1	18.3	14.1
5.03 x 10^5	400	-	-	126	83.8	50.3	25.1
7.85 x 10^5	500	-	-	196	131	78.5	39.3
1.65 x 10^6	725	-	-	-	275	165	82.6
2.46 x 10^6	885	-	-	-	-	246	123
3.14 x 10^6	1000	-	-	-	-	314	157

548

549

550 Table 4. Comparison of volcanic vent sizes on Venus for circular and linear vents and a range of
551 cross sectional vent areas.

A_o [m^2]	r_o [m]	b_o [m]				
		L_o = 200 m	L_o = 500 m	L_o = 1000 m	L_o = 2000 m	L_o = 5000 m
1.26 x 10^3	20	3.14	1.26	0.628	0.314	0.126
2.83 x 103	30	7.07	2.83	1.41	0.707	0.283
7.85 x 10^3	50	19.6	7.85	3.93	1.96	0.785
1.54 x 10^4	70	-	15.4	7.69	3.85	1.54
3.13 x 10^4	100	-	31.4	15.7	7.85	3.14
4.90 x 10^4	125	-	49.1	24.5	12.3	4.91
7.07 x 10^4	150	-	-	35.3	17.7	7.07
1.26 x 10^5	200	-	-	62.8	31.4	12.6
1.59 x 10^5	225	-	-	79.5	39.8	15.9
1.96 x 10^5	250	-	-	95.2	49.1	19.6
2.83 x 10^5	300	-	-	-	70.7	28.3

552

553

554

555 Table 5. Comparison of volcanic vent sizes on Mars for circular and linear vents and a range of
556 cross sectional vent areas.
557

A_o [m^2]	r_o [m]	b_o [m]				
		L_o = 200 m	L_o = 500 m	L_o = 1000 m	L_o = 2000 m	L_o = 5000 m
849	30	2.12	0.849	0.424	0.212	0.085
3150	100	7.89	3.15	1.57	0.789	0.315
7150	175	17.9	7.15	3.57	1.79	0.715
13700	300	-	13.7	6.83	3.42	1.37
25100	500	-	25.1	12.5	6.27	2.51
37800	700	-	37.8	18.9	9.45	3.78
55700	1000	-	-	27.8	13.9	5.57
59900	1200	-	-	30.0	15.0	5.99

558
559
560

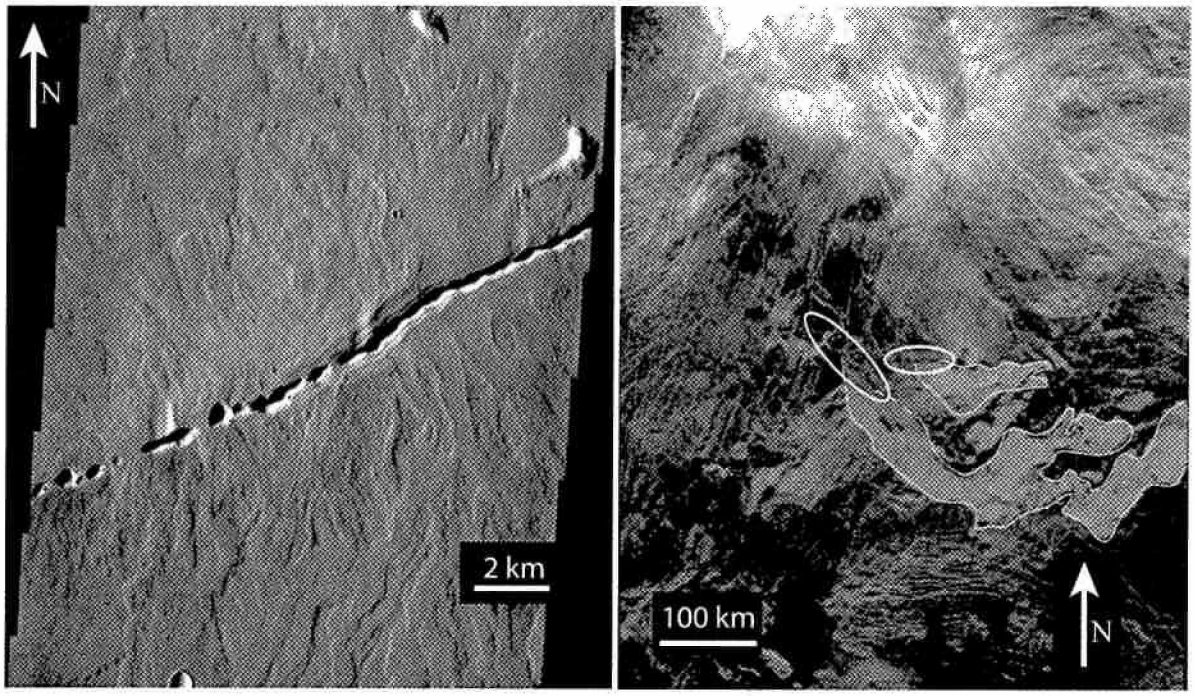

(a) (b)

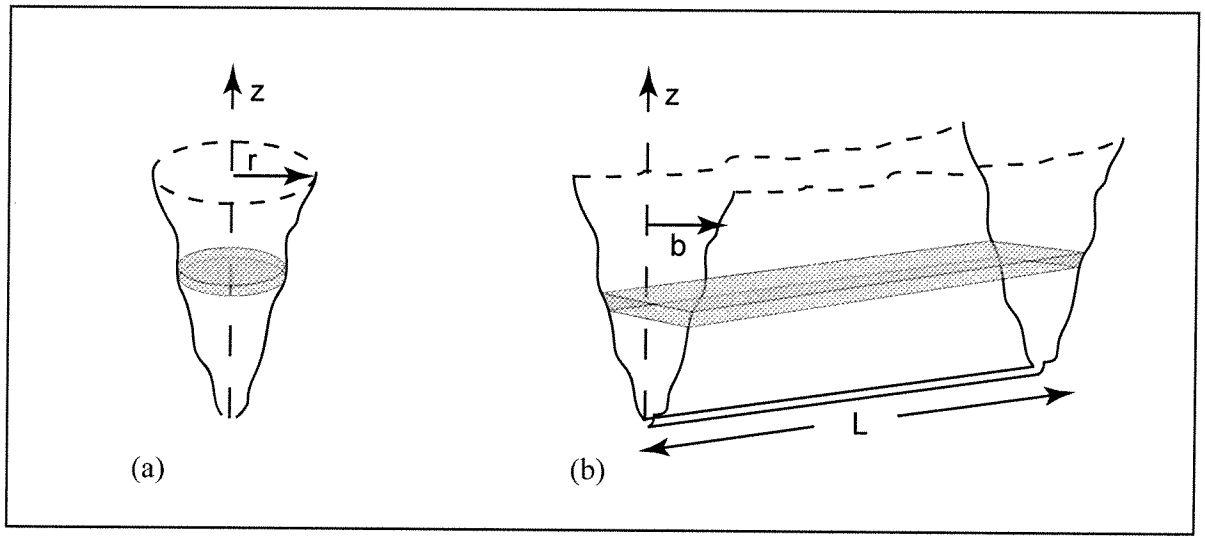
z
r
(a)
z
b
L
(b)

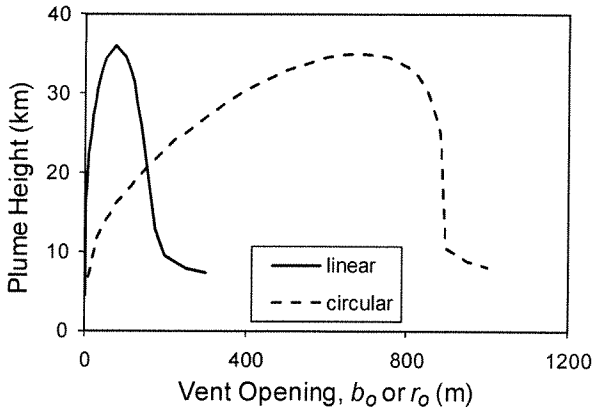
40
30
20
10
0
Plume Height (km)
0
400
800
1200
Vent Opening, b_o or r_o (m)
linear
circular

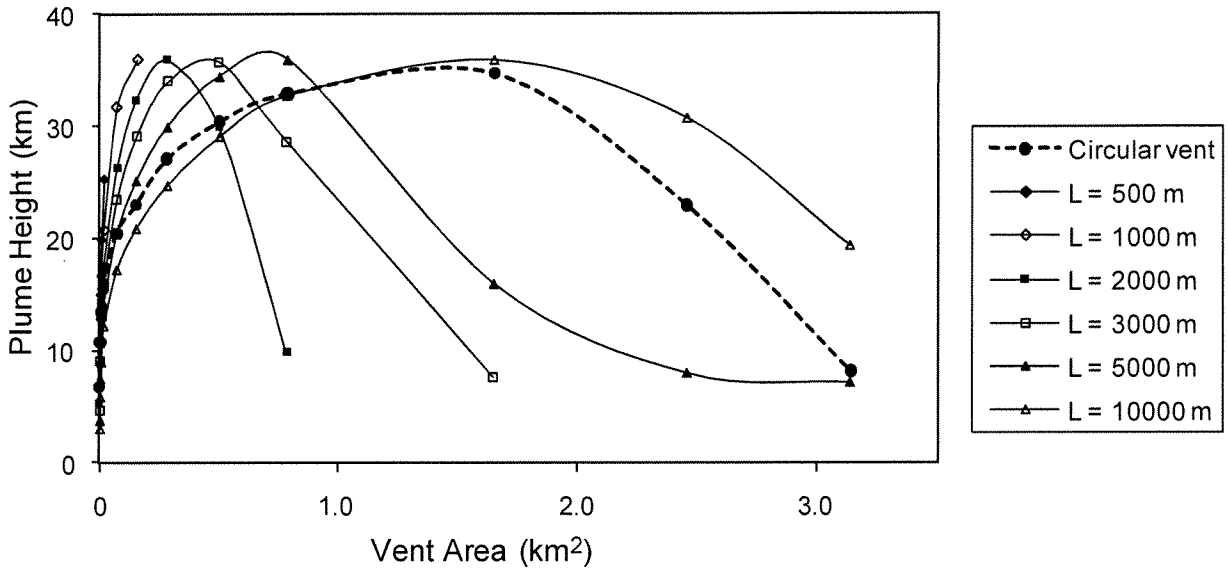
Plume Height (km)
40
30
20
10
0
0
1.0
2.0
3.0
Vent Area (km2)
Circular vent
L = 500 m
L = 1000 m
L = 2000 m
L = 3000 m
L = 5000 m
L = 10000 m

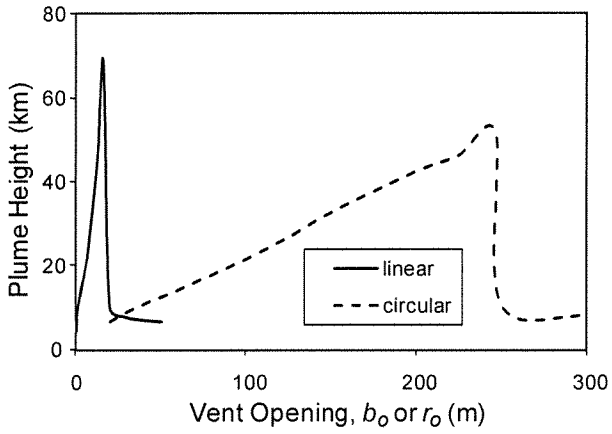
80
60
40
20
0
Plume Height (km)
0
100
200
300
Vent Opening, b_o or r_o (m)
linear
circular

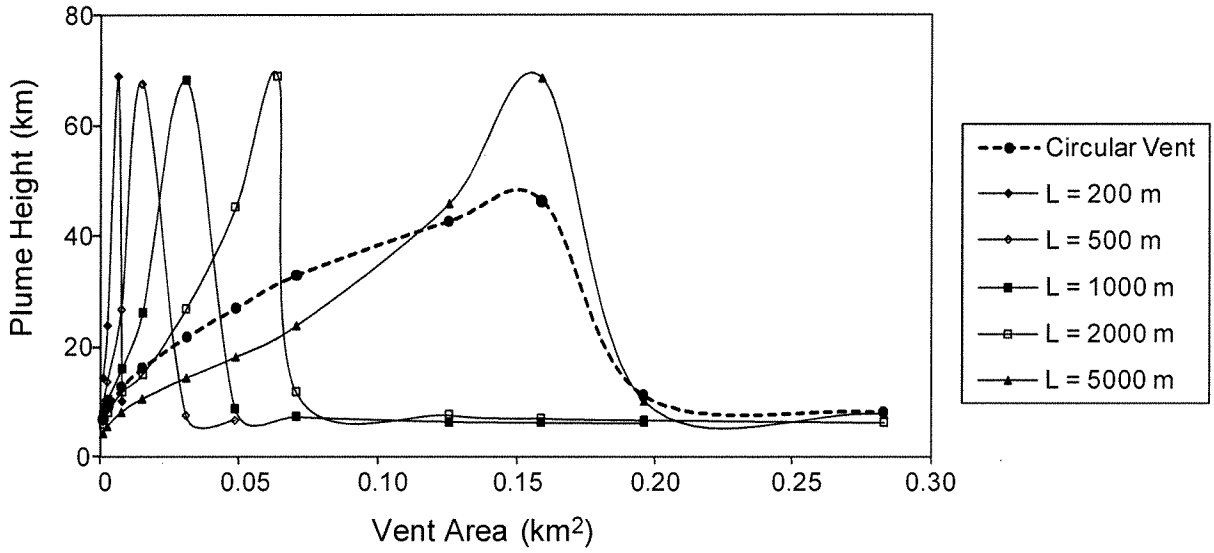
Plume Height (km)
80
60
40
20
0
0
0.05
0.10
0.15
0.20
0.25
0.30
Vent Area (km2)
Circular Vent
L = 200 m
L = 500 m
L = 1000 m
L = 2000 m
L = 5000 m

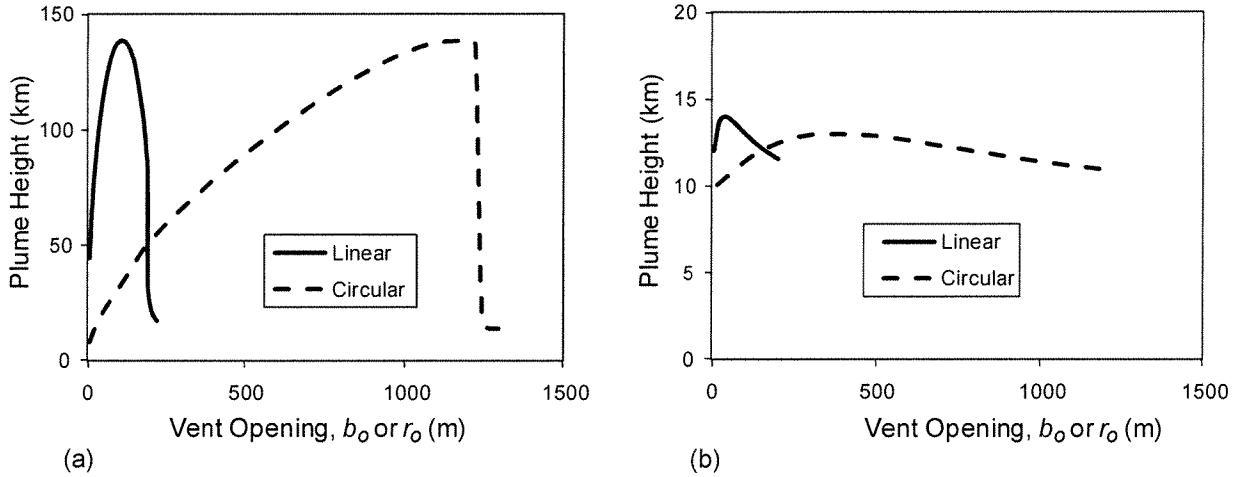
150
100
50
0
Plume Height (km)
0
500
1000
1500
Vent Opening, b_o or r_o (m)
Linear
Circular
(a)
20
15
10
5
0
Plume Height (km)
0
500
1000
1500
Vent Opening, b_o or r_o (m)
Linear
Circular
(b)

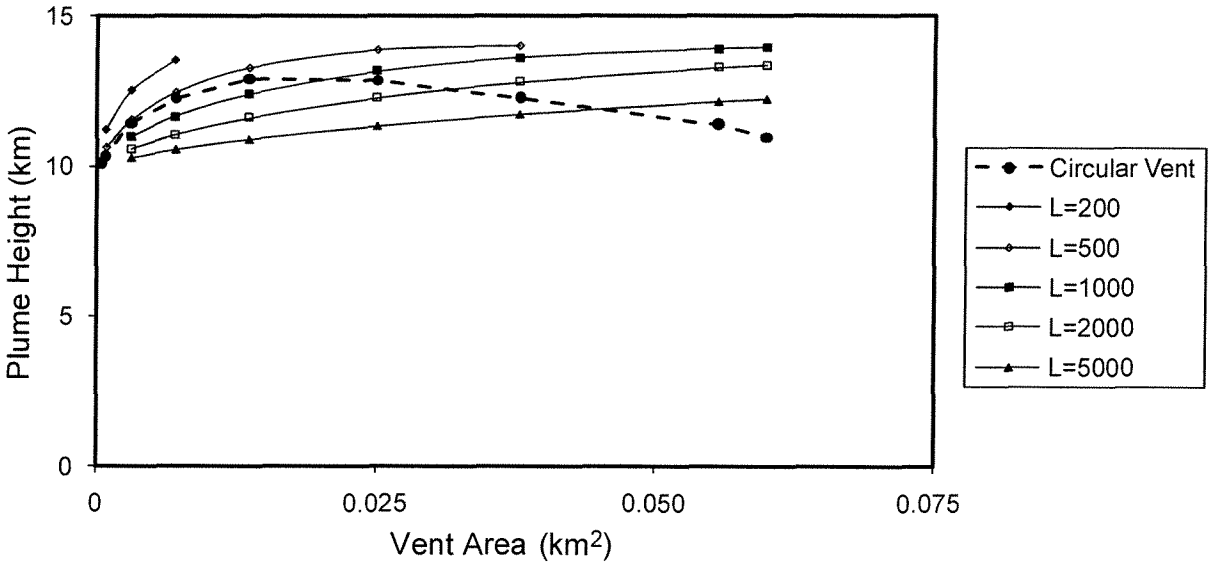
15
10
5
0
Plume Height (km)
0
0.025
0.050
0.075
Vent Area (km2)
Circular Vent
L=200
L=500
L=1000
L=2000
L=5000